Journal of Solid State Chemistry 181 (2008) 2591–2600

Contents lists available at ScienceDirect

Journal of Solid State Chemistry

journal homepage: www.elsevier.com/locate/jssc

The crystal structure, vibrational and luminescence properties of the nanocrystalline $KEu(WO_4)_2$ and $KGd(WO_4)_2$:Eu^{3+} obtained by the Pechini method

L. Macalik [a,*], P.E. Tomaszewski [a], R. Lisiecki [a], J. Hanuza [a,b]

[a] Institute of Low Temperature and Structure Research, Polish Academy of Sciences, P.O. Box 1410, 50-950 Wrocław 2, Poland
[b] Department of Bioorganic Chemistry, Faculty of Industry and Economics, Wrocław University of Economics, ul. Komandorska 118/120, 53-345 Wrocław, Poland

ARTICLE INFO

Article history:
Received 19 November 2007
Received in revised form
9 May 2008
Accepted 8 June 2008
Available online 17 June 2008

Keywords:
Europium potassium double tungstate
Gadolinium potassium double tungstate
Pechini method
Nanocrystals
X-ray
Raman
IR
Size-driven phase transitions

ABSTRACT

The luminescent nanocrystalline $KEu(WO_4)_2$ and $KGd_{0.98}Eu_{0.02}(WO_4)_2$ have been prepared by the Pechini method. X-ray diffraction, infrared and Raman spectroscopy as well as optical spectroscopy were used to characterise the obtained materials. The crystal structure of $KEu(WO_4)_2$ was refined in $I2/c$ space group indicating the isostructurality to $KGd(WO_4)_2$. The size of the crystalline grains depended on the annealing temperature, increasing with the increase of the temperature. The average size of crystallites of both crystals formed at 540 °C was about 50 nm. Vibrational spectra showed noticeable changes as a function of size due to, among others, phonon confinement effect. Luminescence studies did not reveal significant changes for the nanocrystallites with the lowest grain size in comparison with the bulk material. The differences observed in luminescence spectra in form of slight inhomogeneous broadening of the spectral lines and increase of the hypersensitive I_{0-2}/I_{0-1} ratio point to very low symmetry of Eu^{3+} ions and change of the polarisation of the local vicinities of Eu^{3+}. X-ray diffraction, vibrational and optical studies showed that the structure of the synthesised nanocrystalline $KEu(WO_4)_2$ and $KGd(WO_4)_2$:Eu is nearly the same as that found for the bulk material. The size-driven phase transitions were established for both compounds.

1. Introduction

Rare-earth elements form a series of double isomorphous tungstates and molybdates with the general formula $K^{I}Ln^{III}(M^{VI}O_4)_2$, where Ln^{III} is a lanthanide ion and M^{VI} = Mo or W. These materials can be used as laser active media in which the emission properties are modified by the selection of the Ln^{3+} ion and by optimisation of its concentration. $KGd(WO_4)_2$ has been found to be especially promising material for a solid-state Raman laser application [1]. Well-characterised solid-state laser materials are evaluated for performance in optical refrigeration as well as radiation-balanced laser systems. It seems that, for such systems, $KY(WO_4)_2$ and $KGd(WO_4)_2$ are the most promising crystalline hosts for trivalent ytterbium ions [2].

Although properties of crystalline double tungstates and molybdates were a subject of numerous studies, functional electronic device demands the replacement or assembly of nanometre scale components into well-defined structures. In recent years, a rapid development of experiments with nanomaterials takes place due to their existing and future applications in various technological areas [3,4]. The materials with grain size less than 100 nm exhibit different optical, electrical, catalytic and mechanical properties than conventional microcrystalline specimens [5–8]. Therefore, processing techniques that allow production of large quantities of nanomaterials and a more precise control of chemical structures are important area of investigations. In order to examine the chemical and physical properties of nanomaterials, the alternative simple and cost-effective route is required. The Pechini process [9] is such polymeric precursor method known as versatile low temperature route. Among the advantages of this method are high efficiency, short time synthesis and the possibility to prepare complex compositions at a relatively low temperature.

According to the literature data, only three rare earth double tungstates, $NaLa(WO_4)_2$ and $KRE(WO_4)_2$ (RE = Gd and Yb), were prepared in nanocrystalline state so far [10,11]. In this paper, we shall focus attention on $KEu(WO_4)_2$ (KEW) and $KGd(WO_4)_2$:Eu (2 at wt%) (KGEW) prepared by Pechini method in order to investigate their optical properties and study the grain size dependence of their properties. Moreover, to our knowledge, both crystals were not structurally described.

* Corresponding author. Fax: +48 71 344 1029.
E-mail address: l.macalik@int.pan.wroc.pl (L. Macalik).

0022-4596/$ - see front matter © 2008 Elsevier Inc. All rights reserved.
doi:10.1016/j.jssc.2008.06.026

2. Experimental

2.1. Preparation of nanocrystalline powders

The $KEu(WO_4)_2$ and europium(III)-doped $KGd(WO_4)_2$ samples were prepared by the Pechini method. Europium nitrate $Eu(NO_3)_3 \cdot x5H_2O$ (Alfa Aesar, 99.99%), gadolinium nitrate $Gd(NO_3)_3 \cdot xH_2O$ (Alfa Aesar, 99.99%), potassium tungstate K_2WO_4 (Alfa Aesar, 99.5%) and ammonium metatungstate $(NH_4)_6W_{12}O_{41}$ (Fluka) were used as source of metallic cations. First, 1.46 mmol of the europium nitrate or 1.42 mmol of the gadolinium and 0.03 mmol of the europium nitrates and, separately, 0.72 mmol of the potassium and 0.18 mmol of the ammonium tungstates were dissolved in distilled water. Separately, 35 mmol of the citric acid was dissolved in distilled water in order to obtain the molar ratio of citric acid to total cations as 15:1. Next one-half of the aqueous citric acid solution was added to the nitrate solution and another half was added to the tungstate solution. After complete homogenisation, both solutions were mixed together. The formation of complex ring-shaped compounds around the metal cations takes place in the solution. Metals ions are chelated by the carboxyl groups of the citric acid and remain homogeneously distributed in the solution. To create a rigid polyester net, the appropriate amount of ethylene glycol was added (the molar ratio of the glycol to citric acid was 1:1). The mixture was dried at 80 °C for 20 h with stirring and then heated at 110 °C in air for 5 days. During this time, the solution turned into yellowish gel which expanded several times of its original volume and, in the end, a brown resin was obtained as a result of the whole procedure. The resin was hard and transparent both for the double potassium–europium tungstate and for the double potassium–gadolinium tungstate.

In the next step, the decomposition of the obtained resin was performed. Pieces of the crushed resin were annealed in the air atmosphere at selected temperatures between 500 and 1000 °C for 1 h to obtain the white nanopowder tungstate. The time and temperature of the annealing procedure determines the size of the grains of desired nanomaterial. Single phases of potassium–europium double tungstate and potassium–gadolinium double tungstate with different crystallite sizes were the only final products for the temperatures exceeded about 550 °C. When the annealing temperature is lower, the polymeric decomposition is not complete and residual organic molecules are still present.

2.2. Experimental techniques

X-ray powder diffraction patterns were recorded at room temperature by using STADI-P powder diffractometer (STOE, Germany) working in the transmission geometry and equipped with a linear 140°-PSD detector. Cu$K\alpha_1$ radiation in the 2Θ range from 3.0° to 90.0° with a step of 0.03° was used.

The crystal structure analyses were made by the Rietveld method with the FullProf program using the profile function of pseudo-Voigt with axial divergence asymmetry [12,13]. The effective 2Θ-range was limited to 10–70°.

The average grain size was evaluated from the full width at half maximum (FWHM) of the diffraction peak using the Scherrer equation, which assumes the small crystallite size to be the only cause of X-ray line broadening [14–16]:

$$D = \frac{K\lambda}{\beta \cos \Theta}, \quad (1)$$

where D is the diameter of the crystallite (in the approximation of a spherical shape), λ is the X-ray wavelength (1.54056 Å), β is the FWHM of the diffraction line (in radians), Θ is the Bragg angle of diffraction peak, and the Scherrer constant K is conventionally set to 1.0 [17–21]. The contribution from instrumental broadening was removed by subtracting the FWHM of the corresponding line of well-annealed, bulk crystal using the Halder–Wagner parabolic approximate relation:

$$\beta = \frac{B - b^2}{B}, \quad (2)$$

where β is the FWHM of the true diffraction profile, B and b are the measured FWHM of the equivalent diffraction lines in the specimen and the reference (bulk) sample, respectively [17,20,22–24].

Vibrational spectra of the europium and gadolinium double tungstates were measured at room temperature as a function of the annealing temperature. Infrared spectra were measured with a Biorad 575C FT-IR spectrometer in KBr pellet for the 4000–400 cm^{-1} region and in Nujol suspension for the 500–50 cm^{-1} region. FT-Raman spectra were measured using Bruker RFS 100/S Raman spectrometer with the back scattering arrangement. The 1064 nm line of Nd:YAG laser was used as an excitation source. Signal detection was performed with an InGaAs detector. Both IR and Raman spectra were recorded with a spectral resolution of 2 cm^{-1}.

Optical spectra were recorded at ambient temperature. Reflection spectra were measured using a Cary 5E spectrophotometer with the Praying Mantis diffuse reflectance accessory. The resolution was 0.5 nm. Both the excitation and emission spectra were recorded using a Dongwoo Optron Model DM 711 spectrofluorymeter (South Korea), the spectral resolution of this apparatus was approximately of 0.5 nm. Scanning system consisted of 10 W xenon lamp as the excitation source and coupled with an excitation monochromator with 150 mm focal length and emission monochromator having 750 mm focal length was equipped with a photomultiplier and an InGaAs detector. The emission signal collected was very strong and measurements were not required any correction for the diffraction grating of the monochromator. Excitation spectra in the UV and visible region were corrected with emission spectra of the ozone-free Xe lamp.

3. Results and discussion

3.1. X-ray diffraction studies

The X-ray diffraction patterns for some annealing temperatures of the precursor are shown in Fig. 1. When the temperature was below 540 °C (not showing in Figure), only a mixture of oxide compounds was obtained. At 540 °C, the crystallisation of single phase KEW or KGEW begins because most of the diffraction patterns are sharp and intense. However, the residual organic molecules are still present. The annealing at higher temperature gives rise to crystals of pure phase tungstates with desired composition.

All powder diagrams show the diffraction lines corresponding to the reference crystal structure of $KGd(WO_4)_2$ [25,26]. Therefore, as the crystal structure of $KEu(WO_4)_2$ is not studied yet, we decided to solve them using the powder sample prepared from single crystal. The structure was successfully refined using the atomic parameters from $KGd(WO_4)_2$ crystal as the starting data [25,26]. Both crystals are fully isostructural. In the refinement, we used a non-standard setting $I2/c$ of the recommended $C2/c$ space group [27]. The atomic coordinates are given in Table 1 and selected interatomic distances in Table 2. Fig. 2 shows the final Rietveld plot with a good agreement between the observed and the calculated patterns. Similar structure refinements were made

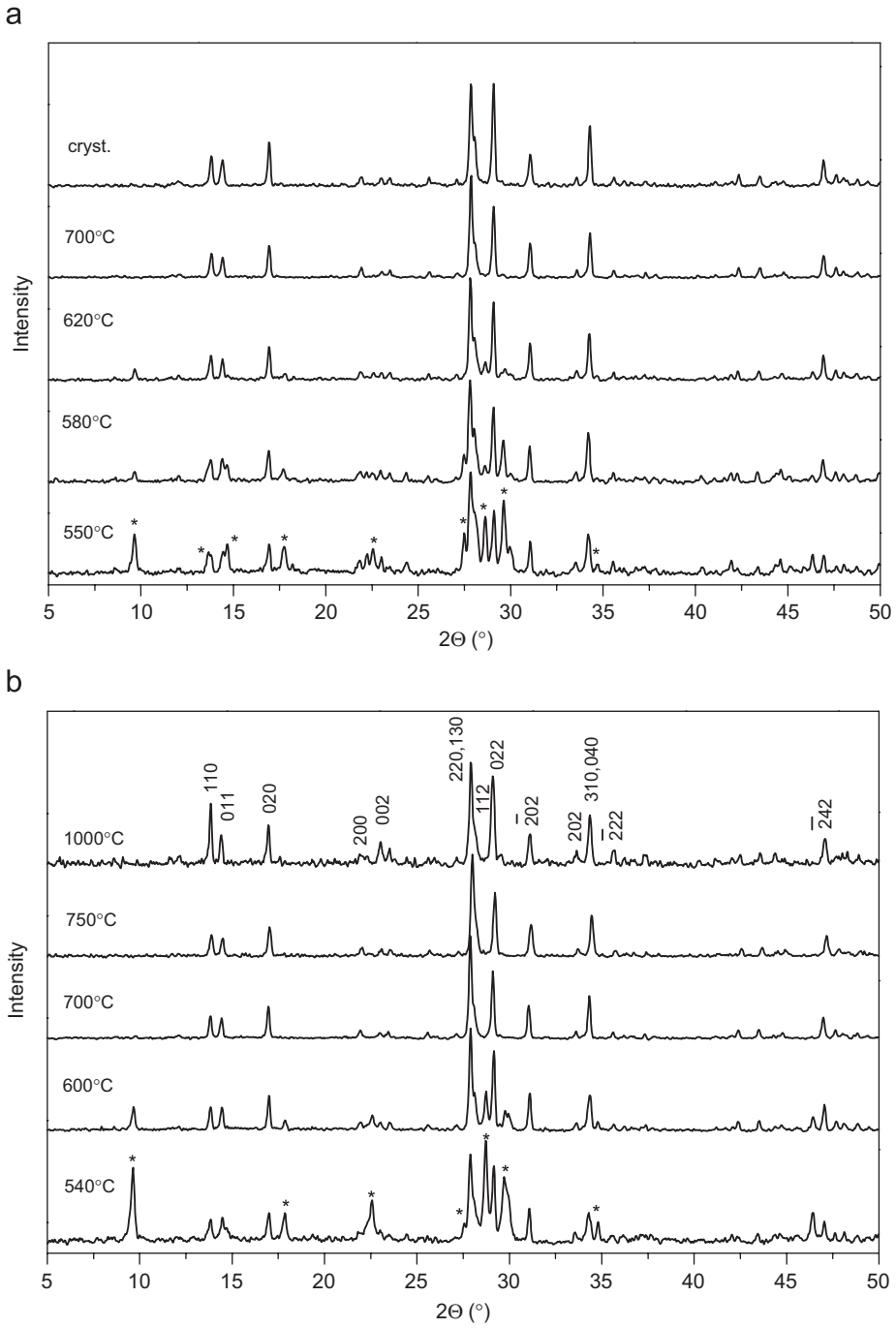

Fig. 1. X-ray powder diffraction pattern of $KEu(WO_4)_2$ samples (a) and $KGd(WO_4)_2$:Eu (b) annealed at several temperatures. The pattern of the bulk sample (denoted as "cryst.") is also presented for comparison. The asterisks show new peaks due to the size-induced phase transition.

Table 1
Refined structural parameters for $KEu(WO_4)_2$ at room temperature, space group $I2/c$, $a = 8.1146(7)$ Å, $b = 10.4496(9)$ Å, $c = 7.5963(5)$ Å, $\beta = 94.349(5)^\circ$, $Z = 2$, $R_p = 9.36$, $R_{wp} = 11.7$, $R_{Bragg} = 7.46$

Atom	Wyckoff position	x	y	z	B_{izo}
K	4*e*	0.5	0.799(4)	0.75	3.5
Eu	4*e*	0.5	0.229(1)	0.75	2.5
W	8*f*	0.693(1)	0.504(1)	0.459(1)	0.5
O1	8*f*	0.887(5)	0.435(5)	0.501(7)	2.0
O2	8*f*	0.527(8)	0.401(4)	0.534(7)	1.0
O3	8*f*	0.749(7)	0.676(5)	0.340(6)	2.0
O4	8*f*	0.695(6)	0.433(3)	0.235(7)	1.0

for KEW crystals annealed at 700 and 650 °C showing again their mutual isostructurality.

The structure of $KEu(WO_4)_2$ consists of a double chains along the *c*-axis formed by WO_6 polyhedra sharing edges and linked by a common vertices. K^+ and Eu^{3+} ions occupy the positions between tungstate octahedra. Their coordinations are 12 and 8, respectively.

However, at least 13 new supplementary diffraction lines appeared for powder diagrams of KEW samples annealed below 640 °C (see Table 3 and Fig. 3). These strong lines indicate a creation of a new phase of KEW slightly different from that known from single crystal studies. This can be explained, for example, as

an appearance of some kind of superstructure (multiplication of the basic unit cell). Unfortunately, the attempt to solve the crystal structure of this new, previously unknown phase of KEW, was unsuccessful. The indexing of powder diagram gave the monoclinic lattice parameters: $a = 15.560(8)$ Å, $b = 12.795(6)$ Å, $c = 9.537(6)$ Å and $\beta = 106.49(5)^\circ$. It should be stressed that these supplementary lines are not come either from the amorphous organic residue or other compounds of different chemical composition. All lines in the XRD diagrams for $KEu(WO_4)_2$ and $KGd(WO_4)_2$:Eu nanopowders could be indexed. In the case of multicomponent mixture of compounds, it could not be possible the reasonable indexing for all lines. So the stoichiometry of obtained compounds is agreed with desired one and another stoichiometry is not present. The effect mentioned above is attributed to the well-known size-driven phase transition [28–30] occurring in KEW annealed at about 640 °C.

The similar situation was observed for $KGd(WO_4)_2$:Eu for annealing temperatures below about 700 °C. It should be as well considered as the size-driven phase transition (Table 3). However, the relative intensity of several diffraction lines recorded for samples annealed at different temperatures are not the same suggesting the existence of an intermediate phase at the temperatures 580 and 600 °C (see Fig. 4). In the case of KEW, this additional behaviour was not observed.

The calculations of grain size were made using *110* and *130* lines for KEW and *100*, *020* and *022* for KGEW samples. The difference in grain size observed for the given temperature of annealing indicates on the deviation from spherical shape of the grains. The average size of crystallites ranges from about 50 nm, for the samples annealed at 540 °C, to about 140 nm for the samples annealed at 750 °C in the case of KGEW and about 500 nm in the case of KEW (Table 4). For KEW, the grains grow more rapidly with the annealing temperature and exceed the nanocrystalline limit just above 550 °C, while for KGEW, this occurs at higher temperatures. This indicates the strong influence of the Eu^{3+} ions doping on the threshold temperature of nanocrystals growth in the Pechini method (deplacing toward lower temperature).

Table 2
Selected interatomic distances (in Å)

W–O1	1.741
W–O2	1.843
W–O2	2.045
W–O3	2.082
W–O4	1.860
W–O4	2.194

Table 3
Selected diffraction lines for $KEu(WO_4)_2$ and $KGd(WO_4)_2$:Eu annealed at 540 and 700 °C

$KEu(WO_4)_2$		*hkl*	$KGd(WO_4)_2$:Eu	
2Θ at 540 °C	2Θ at 700 °C		2Θ at 540 °C	2Θ at 700 °C
9.649	–	100	9.636	–
13.667	–	–	13.649	–
13.792	13.816	110	13.832	13.823
14.420	14.422	011	14.473	14.432
14.659	–	–	14.709	–
16.913	16.928	020	17.008	16.964
17.704	–	–	17.719	–
17.772	–	–	17.864	–
21.818	21.928	200	21.870	21.936
22.228	–	–	22.282	–
22.562	–	–	22.565	–
22.998	23.033	−121	23.040	23.000
24.380	–	–	24.450	–
27.480	–	–	27.543	–
27.831	27.857	130, 220	27.881	27.887
28.048	28.088	112	28.111	28.099
28.222	–	–	28.298	–
28.607	–	–	28.726	–
29.076	29.085	022	29.162	29.106
29.604	–	–	29.725	–
30.004	–	–	29.950	–
31.032	31.060	−202	31.078	31.045

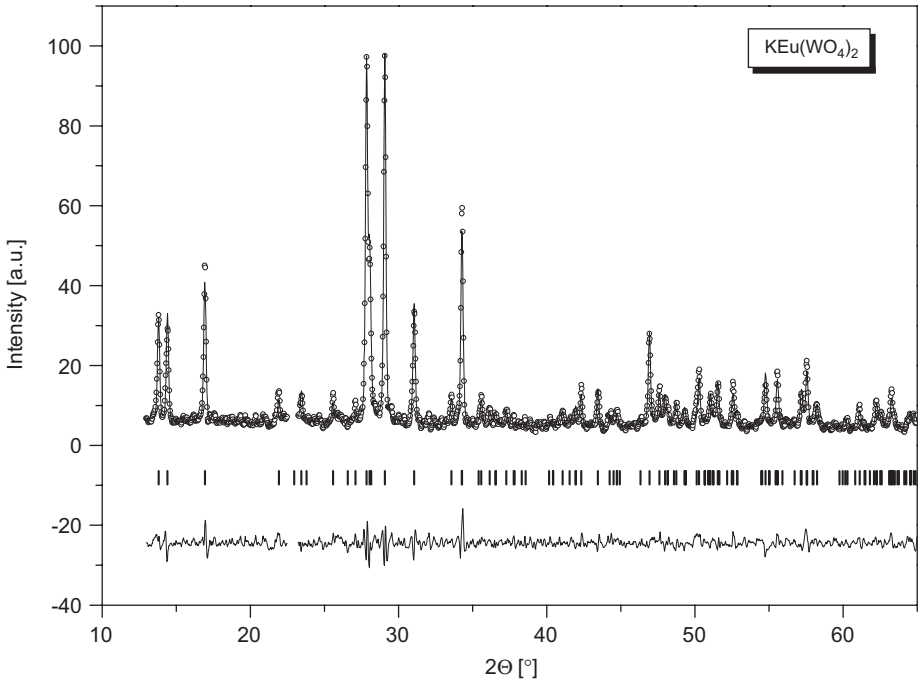

Fig. 2. Final Rietveld plot for $KEu(WO_4)_2$. Small circles (○) correspond to experimental values, and the continuous lines are the calculated pattern; vertical bars (|) indicate the position of Bragg peaks. The bottom trace decepits the difference between the experimental and calculated intensity values.

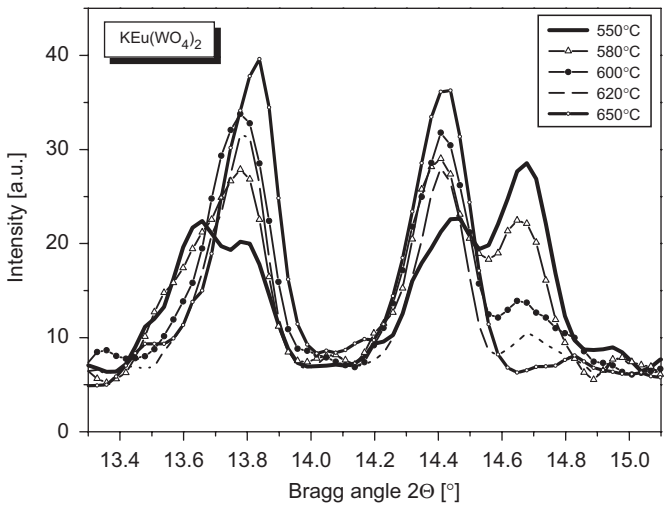

Fig. 3. Selected diffraction lines for $KEu(WO_4)_2$ samples annealed at different temperatures.

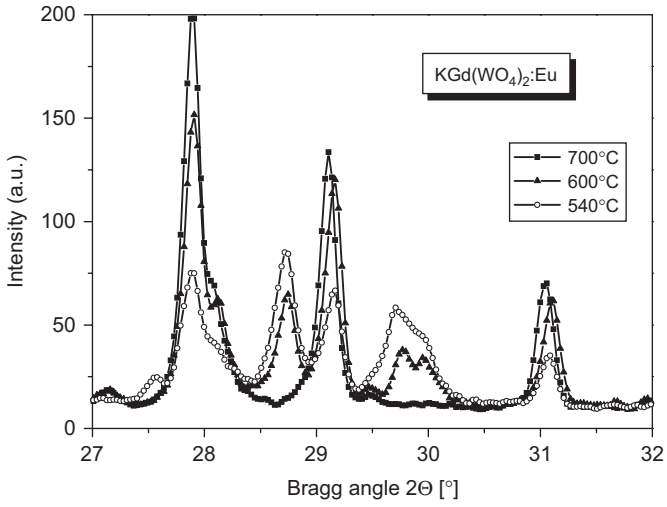

Fig. 4. Selected diffraction lines for $KGd(WO_4)_2$:Eu samples annealed at temperature corresponding to the three observed phases.

Table 4
Calculated average size of crystalline grains as a function of annealing temperature for $KEu(WO_4)_2$ and $KGd(WO_4)_2$:Eu

$KEu(WO_4)_2$		$KGd(WO_4)_2$:Eu	
Annealing temperature (°C)	Crystallite size (nm)	Annealing temperature (°C)	Crystallite size (nm)
540–550	40–80	540–550	50–90
580–620	130–430	580–600	60–130
650–700	220–500	700–750	140

3.2. Vibrational studies

Vibrational spectra of europium and gadolinium nano- and submicrocrystalline tungstates were measured at room temperature as a function of the annealing temperature. Infrared spectra of KEW and KGEW samples are shown in Figs. 5 and 6, respectively. Figs. 7 and 8 present corresponding Raman spectra. The Raman spectra for samples annealed at temperatures up to 540 °C for KEW and 550 °C for KGEW have a high level of the background and bands are rather weak and broad. The spectra of the samples annealed at temperatures higher than 550 °C are free of contribution from the organic components. The background is low and the bands become sharper and more intense. They are very similar each to other and do not exhibit any significant differences as a function of annealing temperature. These spectra contain intense peaks typical for double tungstates and they are also nearly identical with those of the bulk materials. The presence of bands characteristic for the monoclinic double potassium–gadolinium tungstate, $KGd(WO_4)_2$, implies that the structure of the KEW and KGEW samples does not change significantly even when the grain size decreases to 50 nm. In our previous papers on single crystals of potassium–gadolinium and potassium–europium double tungstates [31–33], a factor group analysis was presented. For KEW and KGEW crystallising in the $I2/c$ structure, the factor group analysis predicts 72 vibrational modes, i.e. 36 Raman-active ($17A_g+19B_g$) and 36 IR-active ($17A_u+19B_u$) modes. In the cited papers, it was shown that the highest wavenumber bands at 890–935 cm^{-1} and about 800 cm^{-1} correspond to stretching vibrations of the short terminal W–O bonds. The corresponding bending vibrations were located at 401 cm^{-1}. The stretching vibrations of the octahedral WO_6 units were shown to appear in the 800–860 cm^{-1}, 710–780 cm^{-1} and 620–680 cm^{-1} regions [31,33]. For these vibrations, strong mixing occurs between all W–O bonds of the WO_6 polyhedron. The bands at 769, 530 and 489 cm^{-1} (A_g) and 789, 671 and 467 cm^{-1} (A_u) originate from vibrations of the longer W–O bonds, which are involved in formation of the $W^{O}_{O}W$ bridge. The corresponding bending vibrations were located at 217–440 cm^{-1}. The translational and librational modes of the WO_6 units were identified in the region below 290 cm^{-1}. The translational motions of the K^+ ions were shown to contribute to the vibrations observed at 371, 235 and 174 cm^{-1} (A_g) and 366, 236 and 192 cm^{-1} (A_u), whereas the Gd^{3+} translations were observed at 174, 149 and 97 cm^{-1} (A_g) and 163, 119 and 98 cm^{-1} (A_u).

The spectra obtained for the KEW and KGEW samples annealed at 1000 °C are almost identical with the corresponding data of the bulk sample and can be used as a reference ones. The spectra of all nanocrystalline samples are very similar what corresponds well to the X-ray diffraction data. However, the influence of the annealing temperature and subsequent change of the grain size can be noticed in the vibrational spectra. For instance, several IR modes exhibit shifts towards lower wavenumbers for the nanocrystalline material in comparing to the bulk material. These shifts are observed for KGEW especially for the 115 cm^{-1} ($\Delta\nu = 1\ cm^{-1}$), 242 cm^{-1} ($\Delta\nu = 2\ cm^{-1}$), 317 cm^{-1} ($\Delta\nu = 3\ cm^{-1}$), 395 cm^{-1} ($\Delta\nu = 2\ cm^{-1}$) and 474 cm^{-1} ($\Delta\nu = 3\ cm^{-1}$) lines. Moreover, clearly visible shoulders on the low wavenumber side of the 145, 281 and 435 cm^{-1} IR bands disappear with the decrease of the annealing temperature and bandwidth of the observed bands markedly increases. In the case of KEW, the situation is different. The small shifts towards lower wavenumbers appear for the 144, 349 and 426 cm^{-1} lines but for 316, 466, 832 and 924 cm^{-1} lines the shifts towards higher wavenumbers are observed. The evolution of the IR modes for KEW is presented in Fig. 9.

It is worth to note that for the samples annealed below 600 °C new IR bands appear at 690, 950 and 975 cm^{-1} for KEW and at 693, 947 and 973 cm^{-1} for KGEW (Figs. 5 and 6). Additional bands appear also in the Raman spectra at 322, 405, 586, 730, 819, 879, 912 and 957 cm^{-1} for KEW and at 796, 882 and 957 cm^{-1} for KGEW (Figs. 7 and 8). The modes above 910 cm^{-1} can be attributed to vibrations of the terminal (short) W═O bonds and the bands near 586 and 690 cm^{-1} to stretching vibrations of some tungsten–oxygen bridges [34–37]. Recent studies of WO_3 oxide revealed that modes above 900 cm^{-1} can appear for small crystallites (much smaller than 35 nm) as a result of large concentration of surface atoms [38]. In the case of KEW and KGEW samples, the appearance of these modes due to vibrations

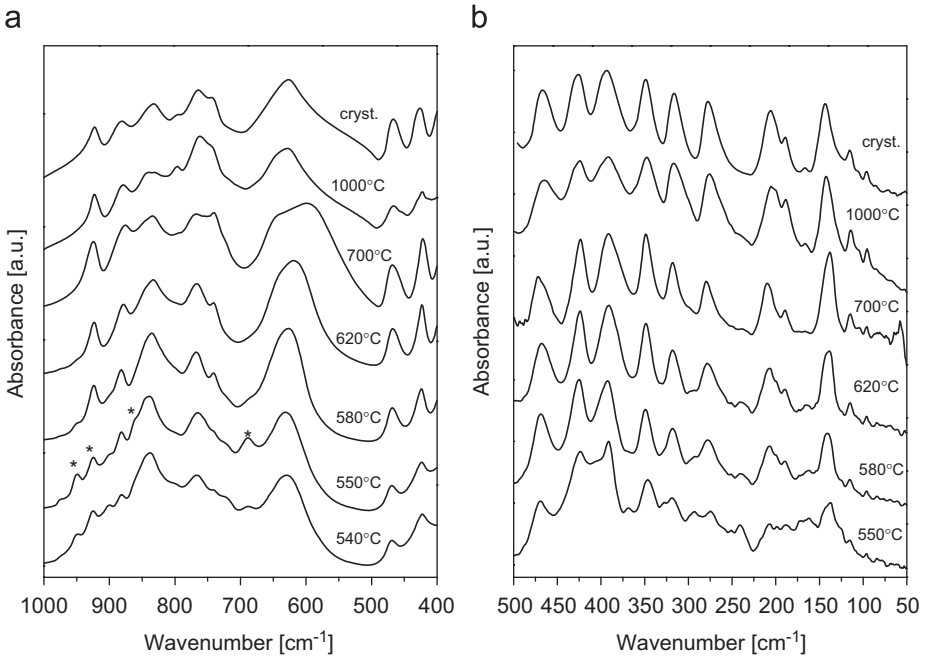

Fig. 5. The evolution of mid-IR (a) and far-IR (b) spectra with the annealing temperature for $KEu(WO_4)_2$. The pattern of the bulk sample (denoted as "cryst.") is also presented for comparison. The asterisks indicate new peaks appearing at low temperature.

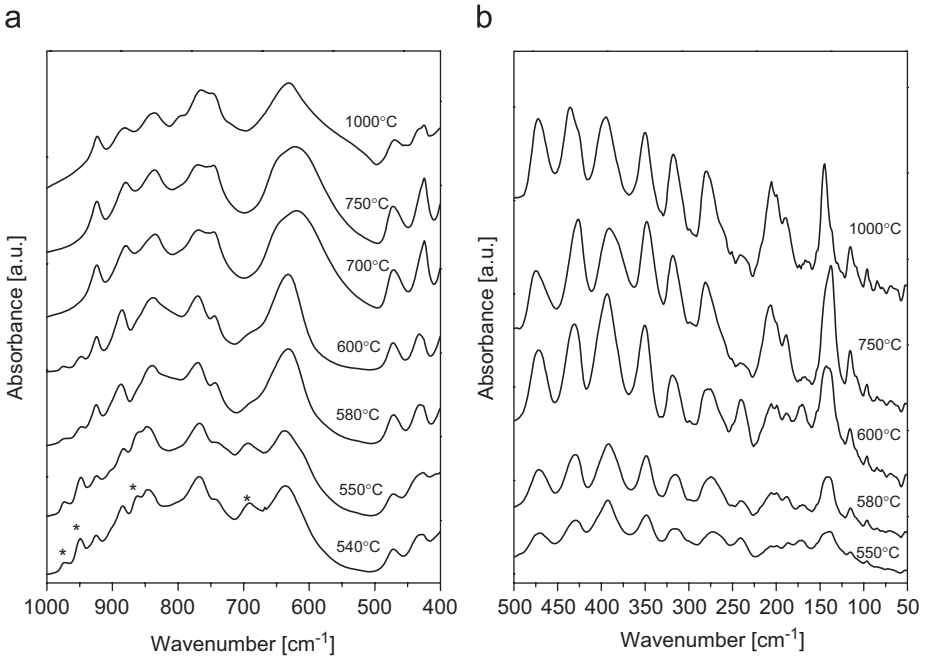

Fig. 6. The evolution of mid-IR (a) and far-IR (b) spectra with the annealing temperature for $KGd(WO_4)_2$:Eu. The pattern of the bulk sample (denoted as "cryst.") is also presented for comparison. The asterisks indicate new peaks appearing at low temperature.

of the surface atoms seems to be not very likely since the size of the crystallites is larger than 50 nm. Moreover, the appearance of these modes is correlated with appearance of the modes near 586 and 690 cm^{-1}, as well as the presence of the additional diffraction lines. We may suppose, therefore, that these high wavenumber modes appear due to presence of new unidentified phase of both compounds.

Apart from appearance of some additional bands, one can notice some visible modification in the shape, intensity or position of certain bands. One can consider the other explications of the observed shift towards lower wavenumbers and broadening of the Raman lines—like phonon confinement, residual stress and defect scattering [39–43]. When the particle size decreases, the stress on the surfaces of particles becomes larger and, finally, it can act on atoms inside particles and produce an additional effect on the balance of short- and long-range forces. The comparison of the full width at half maximum of the Raman bands shows noticeable increase of line widths with the decrease of annealing temperature for KGEW due to the decrease of the grain size. Similar behaviour, although less clearly, is observed for KEW. In this case, the decrease of FWHM in the 620–580 °C range of annealing temperature is observed. Changes of the wavenumber

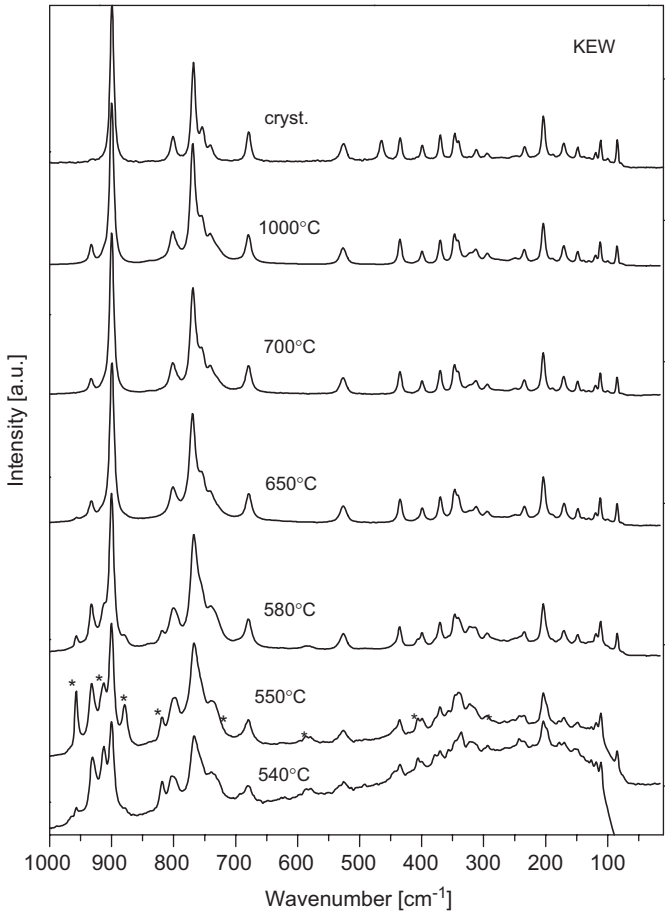

Fig. 7. The evolution of Raman spectra with the annealing temperature for $KEu(WO_4)_2$. The asterisks indicate new peaks appearing at low temperature.

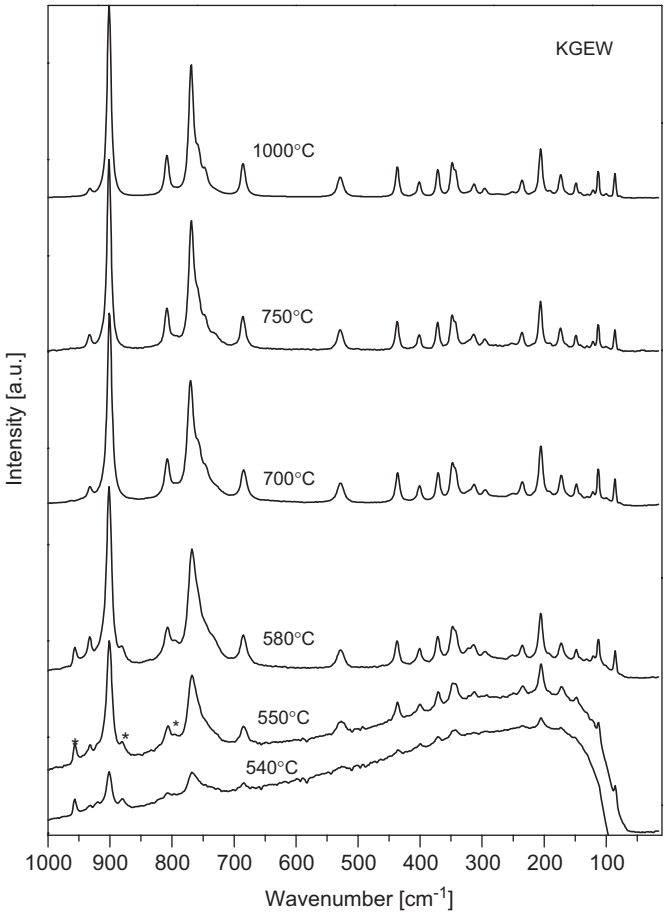

Fig. 8. The evolution of Raman spectra with the annealing temperature for $KGd(WO_4)_2$:Eu. The asterisks indicate new peaks appearing at low temperature.

and the full widths at half maximum are influenced among other things by surrounding lattice defects [44]. The changes visible in our vibrational spectroscopic results indicate that the crystal symmetry is modified by the annealing temperature, i.e. by particle size. It can be concluded that another type of structure appears for nanotungstates, slightly different from that known for single crystal. The existence of such intermediate phase is suggesting by our X-ray studies.

3.3. *Optical studies*

The absorption measurements of nanocrystalline KEW and KGEW samples appeared difficult to realise. Because in absorption spectra the intensity of $4f^6$–$4f^6$ transitions of the Eu^{3+} was too low to observe, the reflectance spectra were measured. The charge transfer (CT) band located at 270 nm dominates the spectra. The absorption transitions from the ground $^7F_0$ level to $^5D_2$ (467 nm), $^5D_1$ (534 nm), $^7F_6$ (1900–2300 nm) and $^7F_5$ (2500–2700 nm) levels become noticeable. They were still very weak and could not form the comparative material. Therefore, the excitation measurements were done. The excitation spectra reflect the transitions of Eu^{3+} ion. Transitions of trivalent gadolinium ion are absence in the visible region because of the large energy gap ($\sim$32,000 cm^{-1}) between the $^8S_{7/2}$ ground level and first $^6P_{7/2}$ excited level. The excitation spectra of KEW and KGEW compounds were obtained in the spectral range between 250 and 580 nm by monitoring the emission of the $^5D_0 \rightarrow {}^7F_2$ transition at 612 nm. They are nearly identical in relation to band positions, their shape and number of components. The spectra for $KEu(WO_4)_2$ annealed at 650 and

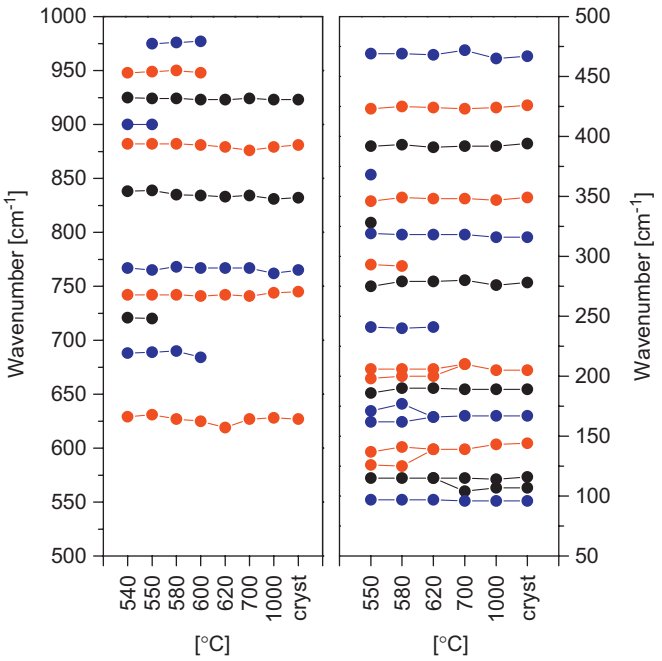

Fig. 9. Annealing temperature (or particle size) dependence of the infrared phonon modes for $KEu(WO_4)_2$ in the frequency range 50–1000 cm^{-1}.

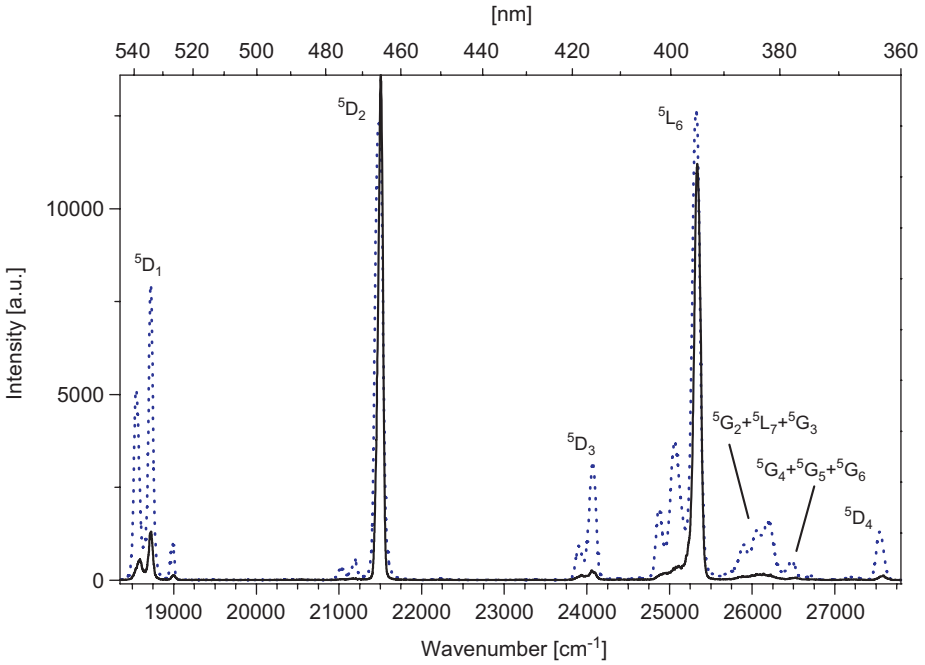

Fig. 10. Excitation spectra of $KEu(WO_4)_2$ annealed at 650 °C (dotted line) and at 540 °C (solid line) by monitoring the emission of the $^5D_0 \rightarrow {}^7F_2$ transition at 612 nm.

450 °C are shown in Fig. 10 where strong bands with sharp peaks corresponding to the $^7F_0 \rightarrow {}^5D_J$, ^5L_J and ^5G_J transitions of Eu^{3+} ion are noticed. Slight shifts of the order of several reciprocal centimetres towards higher energies are visible for peaks originated europium transitions of the sample annealed at 450 °C. It is especially evident for maximums of the $^7F_0 \rightarrow {}^5D_1$ (14 cm^{-1}), $^7F_0 \rightarrow {}^5D_2$ (18 cm^{-1}) and $^7F_0 \rightarrow {}^5L_6$ (16 cm^{-1}).

In order to get additional information on the influence of annealing temperature on the optical properties of the nanocrystalline KEW and KGEW samples, the emission spectra were measured. In general, bands parameters as contour, intensity and distribution are very similar to the spectra of the respective bulk sample [45]. However, we observe some additional inhomogeneous broadening of the spectral lines obtained for the samples annealed at 540 °C. The shifts towards higher energies are also noticeable: 20 cm^{-1} for the $^5D_0 \rightarrow {}^7F_2$ and about 14 cm^{-1} for the $^5D_0 \rightarrow {}^7F_1$ transition. This behaviour indicates that the annealing temperature and, what results from it, the particle size modify the crystal symmetry. Fig. 11 presents the emission spectra of Eu^{3+} for two different annealing temperatures of KEW and KGEW in the 14,000–17,300 cm^{-1} range. The groups of sharp lines in the optical spectra can be attributed to the $^5D_0 \rightarrow {}^7F_{0-4}$ transitions: $^5D_0 \rightarrow {}^7F_1$ (~595 nm), $^5D_0 \rightarrow {}^7F_2$ (~612 nm), $^5D_0 \rightarrow {}^7F_3$ (~650 nm) and $^5D_0 \rightarrow {}^7F_4$ (~703 nm). The emission band reflected the $^5D_0 \rightarrow {}^7F_0$ (580 nm) transition is also observed in the luminescence spectra of $KEu(WO_4)_2$ annealed at 650 °C and $KGd(WO_4)_2$:Eu annealed at 700 °C. And this line is narrow and single what can indicate that europium(III) ions occupy only one site in the chemical environment. However, the intensity of this line is so drastically low that it is difficult to show it in the Figure of luminescence spectra. It is also worth to notice the extremely high intensity of the predominant $^5D_0 \rightarrow {}^7F_2$ transition. The presence of the $^5D_0 \rightarrow {}^7F_{0-4}$ transitions, the J-degeneracy splitting and the positions of the observed bands point to only one low symmetry environment of Eu^{3+} in $KLn(WO_4)_2$ described by one of the following point groups: C_1, C_2, C_{2v} [46].

The intensity of forced electric dipole $^5D_0 \rightarrow {}^7F_2$ transition, named hypersensitive, is strongly sensitive to the nature of the Eu^{3+}-ligand surroundings. It increases as the site symmetry of Eu^{3+} centre decreases. In contrast, the $^5D_0 \rightarrow {}^7F_1$ transition is purely magnetic dipole transition allowed. The ratio between the integrated intensity of these two transitions, $I(^5D_0 \rightarrow {}^7F_2)/I(^5D_0 \rightarrow {}^7F_1)$, is widely used in rare earth systems as a probe of changes on the nature of the cation local surroundings [46–49]. Our studies show that the ratio is 32 and 36 for KEW annealed at 650 and 540 °C, respectively and 26 and 27 for KGEW annealed at 700 and 540 °C, respectively. These values are significantly higher than those observed for Eu^{3+} ions in polyoxomolybdates – about 2.3 [47], $KNbW_2O_9$ – 3.0 [48], titanosilicate – 5.7 [49] or Eu_3BWO_9 – 19.3 [50]. The increase of the hypersensitive I_{0-2}/I_{0-1} ratio was ascribed previously to an increase of both the covalency and the polarisation of the local vicinities of the Eu^{3+} cations (short-range effects) [46,49,51,52]. In the case of KEW and KGEW nanomaterials, where the nanoparticles form loosely packed aggregates, it is difficult to say that changes of the Eu^{3+}-ligand covalency are significant. On the other hand, a greater ratio may correspond to a more distorted (or asymmetric) local cation environment. It could testify that Eu^{3+} posses only C_1 symmetry instead of C_2 symmetry what takes place in bulk material [32]. The local structure of the Eu^{3+} centres in the nanocrystals is nearly the same what is confirmed by the small difference in position of spectral lines for the micron and nanometre-sized particles. It seems that the differences observed in the optical spectra of our nanomaterials could be explained by considering some changes in polarisability of the medium surrounding the nanoparticles.

4. Conclusions

Nanocrystalline double tungstates $KEu(WO_4)_2$ and $KGd(WO_4)_2$:Eu were prepared by the Pechini method. The smallest size of crystallites is of about 50 nm. For KEW, the average size of nanoparticles increases rapidly with the annealing temperature and exceeds the nanocrystalline limit just above 550 °C. Therefore, the strong influence of the Eu^{3+} ions doping on

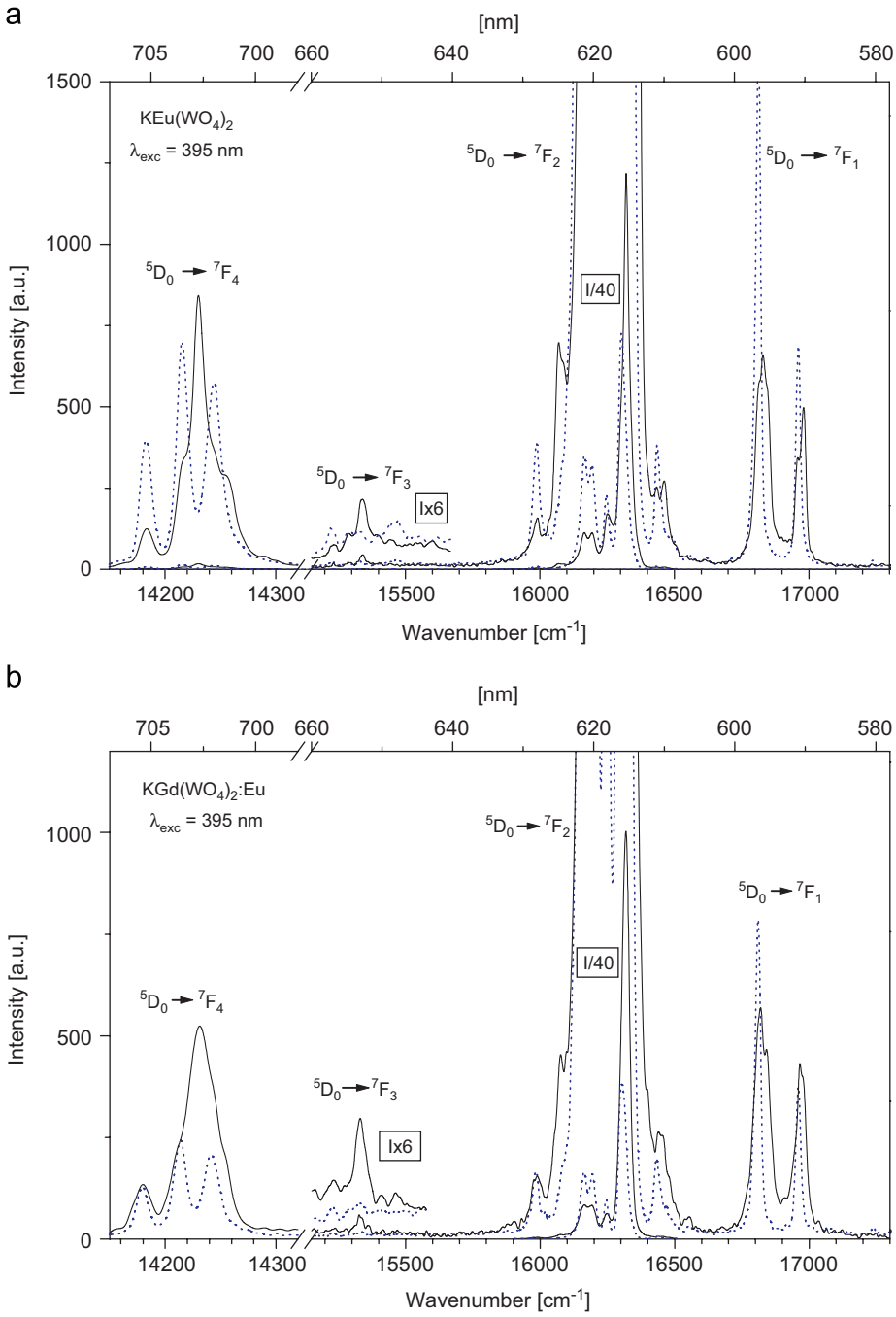

Fig. 11. Emission spectra of $KEu(WO_4)_2$ annealed at 650 °C (dotted line) and at 540 °C (solid line) (a) and of $KGd(WO_4)_2$:Eu annealed at 700 °C (dotted line) and at 540 °C (solid line) (b).

the threshold temperature of nanocrystals growth in the Pechini method is observed.

X-ray diffraction, vibrational and optical studies showed that the structure of the synthesised nanocrystalline $KGd(WO_4)_2$:Eu and $KEu(WO_4)_2$ is nearly the same as that found for the bulk material. The size-induced phase transitions were observed in both compounds.

Some explanations of the observed changes in the vibrational and luminescence spectra were proposed for studied nanocrystals. The complete knowledge of the size effect nature is still indispensable what requires further investigations on technologies of the best quality nanocrystallites preparation and characterization.

Acknowledgments

This work was supported by Ministry of Science and Higher Education in the frame of grant No. 1 PO3B 078 29. The authors would like to thank E. Bukowska for the X-ray diffraction measurements.

References

[1] J.T. Murray, W.I. Austin, R.C. Powell, Adv. Solid State Lasers 19 (1998) 249.
[2] S.R. Bowman, C.E. Mungan, Appl. Phys. B 71 (2000) 807–811.
[3] A.A. Sirenko, J.R. Fox, I.A. Akimov, X.X. Xi, S. Ruvimov, Z. Liliental-Weber, Solid State Commun. 113 (2000) 553.

[4] S.C. Tjong, H. Chen, Mater. Sci. Eng. R45 (2004) 1.
[5] I. Kosacki, H.U. Anderson, Encyclopedia of Materials: Science and Technology, vol. 4, Elsevier, New York, 2001, pp. 3609–3617.
[6] I. Kosacki, T. Suzuki, H.U. Anderson, Ph. Colomban, Solid State Ionics 149 (2002) 99.
[7] A.A. Kaminskii, Phys. Status Solidi A 200 (2003) 215.
[8] K. Takaichi, H. Yagi, A. Shirakawa, K. Ueda, S. Hosokawa, T. Yanagitani, A.A. Kaminskii, Phys. Status Solidi A 202 (2005) R1.
[9] M.P. Pechini, US Patent No. 3330697, 11 July 1967.
[10] F. Wang, X. Fan, D. Pi, Z. Wang, M. Wang, J. Solid State Chem. 178 (2005) 825.
[11] M. Galceran, M.C. Pujol, M. Aguiló, F. Díaz, J Sol–Gel. Sci. Technol. 42 (2007) 79.
[12] T. Roisnel, J. Rodriguez-Carvajal, *WinPLOTR*, a Graphic Tool for Powder Diffraction, version January 2006.
[13] J. Rodriguez-Carvajal, *FULLPROF*: a program for Rietveld refinement and pattern matching analysis, in: Abstracts of the Satellite Meeting on Powder Diffraction of the XVth Congress of IUCr, Toulouse, France, 1990, p. 127.
[14] A.L. Patterson, Phys. Rev. 56 (1939) 978.
[15] A.J.C. Wilson, Proc. Phys. Soc. Lond. 80 (1962) 286.
[16] S.B. Qadri, E.F. Skelton, D. Hsu, A.D. Dinsmore, J. Yang, H.F. Gray, B.R. Ratna, Phys. Rev. B 60 (1999) 9191.
[17] S. Chattopadhyay, P. Ayyub, V.R. Palkar, M. Multani, Phys. Rev B 52 (1995) 13177.
[18] F. Toney, J. Gijo, M. Siby, P.R. Rejikumar, N.V. Unnikrishnan, J. Sol–Gel Sci. Technol. 41 (2007) 163.
[19] J.I. Langford, A.J.C. Wilson, J. Appl. Cryst. 11 (1978) 102.
[20] J.M. Amigó, F.J. Serrano, M.A. Kojdecki, J. Bastida, V. Esteve, M.M. Reventós, F. Marti, J. Eur. Cer. Soc. 25 (1995) 1479.
[21] M. Crosa, V. Boero, M. Franchini-Angela, Clays Clay Miner. 47 (1999) 742.
[22] T.R. Anantharaman, J.W. Christian, Acta Cryst. 9 (1956) 479.
[23] N.C. Halder, C.N.J. Wagner, Acta Cryst. 20 (1966) 312.
[24] H.H. Tian, M. Atzmon, Phil. Mag. A 79 (1999) 1769.
[25] J. Viscakas, I. Mochalov, A. Mikhailov, R. Klevtsova, A. Liubimov, Lietuvos Fizikos Rinkings 28 (1988) 224.
[26] CSD Entry No. 68249, Inorganic Crystal Structure Database, Fachinformationzentrum Karlsruhe, Germany, ver. 1.4.2., 2007.
[27] M.C. Pujol, R. Sole, J. Massons, J. Gavalda, X. Solans, C. Zaldo, F. Diaz, M. Aguilo, J. Appl. Cryst. 34 (2001) 1.
[28] S. Tsunekawa, S. Ito, T. Mori, K. Ishikawa, Z.-G. Li, Y. Kawazoe, Phys. Rev. B 62 (2000) 3065.
[29] G. Baldinozzi, D. Simeone, D. Gosset, M. Dutheil, Phys. Rev. Lett. 90 (2003) 216103.
[30] M. Mączka, K. Hermanowicz, P.E. Tomaszewski, M. Zawadzki, J. Hanuza, Solid State Sciences 10 (2008) 61.
[31] J. Hanuza, L. Macalik, Spectrochim. Acta 43A (1987) 361.
[32] L. Macalik, Polish J. Chem. 69 (1995) 286.
[33] L. Macalik, J. Hanuza, A.A. Kaminskii, J. Raman Spectrosc. 33 (2002) 92.
[34] J. Hanuza, L. Macalik, M. Mączka, E.T.G. Lutz, J.H. van der Maas, J. Mol. Struct. 511 (1999) 85.
[35] M. Mączka, J. Hanuza, A. Majchrowski, J. Raman Spectr. 32 (2001) 929.
[36] M. Mączka, J. Hanuza, A. Waśkowska, J. Raman Spectr. 34 (2003) 432.
[37] M.F. Daniel, B. Desbat, J.C. Lassegues, B. Gerand, M. Figlarz, J. Solid State Chem. 67 (1987) 235.
[38] M. Boulova, G. Lucazeau, J. Solid State Chem. 167 (2002) 435.
[39] K.K. Tiong, P.M. Amirtharaj, F.H. Pollak, D.E. Aspnes, Appl. Phys. Lett. 44 (1984) 122.
[40] P. Parayanthal, F.H. Pollak, Phys. Rev. Lett. 52 (1984) 1822.
[41] M. Holtz, R. Zallen, O. Brafman, S. Matteson, Phys. Rev. B 37 (1988) 4609.
[42] J.W. Ager III, D.K. Veirs, G.M. Rosenblatt, Phys. Rev. B 43 (1991) 6491.
[43] J.E. Spanier, R.D. Robinson, F. Zhang, S.W. Chan, I.P. Herman, Phys. Rev. B 64 (2001) 245407.
[44] Y. Shiratori, A. Magrez, J. Dornseiffer, F.H. Haegel, Chr. Pithan, R. Waser, Phys. Chem. B 109 (2005) 20122.
[45] J. Hanuza, L. Macalik, B. Macalik, W. Stręk, Acta Phys. Polonica A 84 (1993) 899.
[46] L.D. Carlos, A.L.L. Videira, Phys. Rev. B 49 (1994) 11721.
[47] R. Cao, S. Liu, L. Xie, Y. Pan, J. Cao, Y. Liu, Inorg. Chim. Acta 361 (2008) 2013.
[48] L. Macalik, M. Mączka, J. Hanuza, A. Bednarkiewicz, D. Hreniak, W. Stręk, A. Majchrowski, J. Alloys Compd. 380 (2004) 248.
[49] J.P. Rainho, L.D. Carlos, J. Rocha, J. Lumin. 87–89 (2000) 1083.
[50] M. Mączka, P. Tomaszewski, J. Stępień-Damm, A. Majchrowski, L. Macalik, J. Hanuza, J. Solid State Chem. 177 (2004) 3595.
[51] E.W.J.L. Oomen, A.M.A. van Dongen, J. Non-Cryst. Solids 111 (1989) 205.
[52] R. Reisfeld, E. Greenberg, R.N. Brown, M.G. Drexhage, C.K. Jorgensen, Chem. Phys. Lett. 95 (1983) 91.